Biorheology 51 (2014) 275–291
DOI 10.3233/BIR-14009
IOS Press

The characterization of a non-Newtonian blood analog in natural- and shear-layer-induced transitional flow

Lin Li, Andrew M. Walker * and David E. Rival
Department of Mechanical Engineering, University of Calgary, Calgary, AB, Canada

Received 18 February 2014
Accepted in revised form 1 August 2014

Abstract.
BACKGROUND: Although a blood analog of aqueous glycerol and xanthan gum was found to replicate the viscoelastic behavior of blood, measurements were restricted to laminar flow.
OBJECTIVE: To expand the characterization of a non-Newtonian blood analog of aqueous glycerol and xanthan gum to transitional Reynolds numbers to quantify its behavior as a function of both natural and shear-layer-induced mechanisms.
METHODS: A Newtonian analog and a shear-thinning aqueous glycerol, xanthan gum solution were circulated through an *in vitro* flow loop replicating both a straight and obstructed artery where transition was initiated through natural and shear-layer-induced mechanisms respectively. Steady and pulsatile pressure drop measurements for both fluids were acquired across a range of Reynolds numbers up to 7600 and Womersley numbers of 4 and 6.
RESULTS: In steady and pulsatile straight flow, the non-Newtonian analog presented with reduced pressure drops and prolonged laminar flow to Reynolds numbers of 3200 and 3800 respectively. Upon blockage inclusion, non-Newtonian minor losses were comparable to Newtonian in steady flow and greater in pulsatile flow suggesting an elongation of downstream non-Newtonian recirculation. Although non-Newtonian total system pressure drops in both straight and obstructed flows were lower, the ratio of pressure drop difference between the two fluids decreased through shear-layer-induced transition.
CONCLUSIONS: These findings not only demonstrated the suitability of using a xanthan gum analog to model blood flow in transitional regimes, but also presented the respective differences in analog behavior as a function of transition mechanism.

Keywords: Blood analog fluids, viscoelastic fluids, natural transition, shear-layer-induced transition

1. Introduction

In the large arteries of the vasculature, blood is often modeled as a Newtonian fluid under the assumption that the rheological behavior is linear on account of high shear strain rates [1–3]. However, blood displays shear-thinning, non-Newtonian behavior resultant from the viscoelastic properties of red blood cells in plasma. This suggests that the application of a constant viscosity assumption to model low shear strain rate flows distorts true flow behavior. Indeed, studies by Mejia et al. [3], Schirmer and Malek [4],

*Address for correspondence: PhD Andrew Walker, Department of Mechanical Engineering, University of Calgary, 2500 University Dr. N.W., Calgary, Alberta, Canada, T2N 1N4. Tel.: +1 403 210 7593; Fax: +1 403 282 8406; E-mail: walkeram@ucalgary.ca.

Cavazutti et al. [5] and Walker et al. [6,7] have demonstrated that Newtonian assumptions may underestimate wall shear stress (WSS) and wall forces while elongating recirculation in pathological arterial segments.

Although cardiovascular flow is presumed laminar, transitional flow can be promoted by adverse cardiovascular pathologies including stenoses and aneurysms through downstream shear-layer instabilities [8–11]. Depending on the severity of the pathology, downstream transition can be initiated at Reynolds numbers (*Re*) greater than an order of magnitude lower than that under conditions of steady, laminar, straight pipe flow [11]. Furthermore, Stein and Sabbah [11] concluded that turbulence is present in the ascending aorta of normal subjects at times of elevated cardiac output while Vétel et al. [12] noted that blood flow within the carotid may undergo transition on account of its complex geometry. Han et al. [13] demonstrated prolonged laminar behavior of porcine blood to a higher critical *Re* (Re_{crit}), which represents the *Re* at which transition is initiated, in relation to a Newtonian blood analog. This finding supports the inclusion of non-Newtonian viscous assumptions to the modeling of transitional blood flow environments; however, as noted by Walker et al. [7] application of such an assumption has been minimal. Computationally, in a shear-layer-induced transitional environment, Molla and Paul [14] predicted that a non-Newtonian model extended downstream recirculation while dampening turbulent kinetic energy. Comparable findings were measured experimentally by Walker et al. [7]. Despite analogous results between Molla and Paul [14] and Walker et al. [7], caution must be taken in the computational modeling of non-Newtonian transitional flow where resulting flow dynamics are greatly influenced on chosen model parameters [15].

Ideally, whole blood would serve as the circulating fluid for experimental models quantifying transitional flow. However, large quantities would be required necessitating proper safety and handling measures. Additionally, the stability of blood used for *in vitro* testing is often diminished compared to that *in vivo* through alterations to its viscous behavior due to the use of anti-coagulants. Alternatively, Brookshier and Tarbell [16] demonstrated that a non-Newtonian blood analog composed of aqueous glycerol and xanthan gum provided a close match to the viscoelastic behavior of porcine blood across a range of representative hematocrit. However, measurements by Brookshier and Tarbell [15] were restricted to laminar flow. Thus, aqueous glycerol/xanthan gum applicability to modeling transitional blood flow through the demonstration of prolonged laminar flow behavior was not immediately acknowledged. Through pressure drop measurements in steady pipe flow, Walker et al. [7] demonstrated prolonged laminar flow behavior of the xanthan gum analog that was in close agreement with the Re_{crit} measured by Han et al. [13]. However, measurements were restricted to steady pipe flow up to $Re \leqslant 3400$. Further investigations need to be undertaken to assess the performance of the blood analog in more complicated flow conditions.

Building upon the work of Brookshier and Tarbell [16] and Walker et al. [7], the first aim of our study was to expand the evaluation of the xanthan gum blood analog beyond $Re > 3400$ in both steady and pulsatile flow. Through the acquisition of pressure drop measurements on an *in vitro* straight, simplified arterial flow loop, we expect that the non-Newtonian analog in accordance with Walker et al. [7], will delay the onset of natural pipe flow transition to a comparable *Re* in steady flow to that of porcine blood. For pulsatile flows, Trip et al. [17] concluded that *Re* was the sole determinant of transitional onset and neither Womersley number (α) nor oscillatory Reynolds number (Re_{os}) were controlling parameters. However, the work of Trip et al. [17] was restricted to $\alpha \geqslant 10$. Past work has identified an α region between 4 and 8 where uncertainty remains on the relationship between α and the initiation of transition [17,18]. Thus, it was our aim to quantitatively evaluate the relationship between transition and pulsatility within this α range between Newtonian and xanthan gum analog fluids. It is hypothesized that transition

will be delayed for both fluids at higher α as the increased pulsatile frequency will serve to limit the generation of turbulent bursts while the xanthan gum analog will exhibit prolonged laminar flow behavior to a higher Re_{crit} in relation to the Newtonian analog.

To generate shear-layer-induced transitional flow comparable to that created by adverse pathologies, an obstruction (representing a simplified stenosis) was incorporated into the *in vitro* straight flow loop. It was our aim to evaluate obstruction induced pressure drops via shear-layer-induced transition as a function of analog viscous behavior in relation to pressure drops acquired in the straight flow loop. To date, studies quantifying shear-layer-induced transitional flow fields have largely relied on Newtonian assumptions for blood. However, findings by Molla and Paul [14] and Walker et al. [7] have demonstrated alterations to downstream flow fields including elongated recirculation length upon the incorporation of non-Newtonian viscous behavior. Based on the relationship between recirculation length and energy dissipation [19–21], we hypothesize that the ratios of the Newtonian to non-Newtonian shear-layer-induced pressure drops are lower in comparison to the same ratio in the straight flow loop on account of elongated non-Newtonian recirculation length.

2. Methods

2.1. Characterization of working fluids

The working fluids included a Newtonian blood analog consisting of 12% by weight aqueous glycerol and a non-Newtonian analog of 50 mg xanthan gum dissolved in 1450 ml of 4% by weight aqueous glycerol. The dynamic viscosity of the Newtonian control fluid was taken as the average of three measurements acquired by a Cannon-Fenske routine calibrated CRFC (9271-B50) series size-50 capillary viscometer (Cannon-Fenske, PA, USA) with water as the control fluid at room temperature (20°C). The densities of the Newtonian and non-Newtonian analog fluids were 1026 kg/m^3 and 1009 kg/m^3, respectively.

Prior to measurements, the rheological behavior of the analog fluids were characterized through pressure drop measurements in steady laminar flow through a 0.635 cm diameter (D) acrylic pipe across a distance of $263D$. Both fluids were subjected to identical flow rates. To account for the larger near-wall shear strain rate for the non-Newtonian fluid, the Weissenberg–Rabinowitsch correction (Eq. (1)) for wall shear strain rate was applied [22]:

$$\gamma_{\text{c}} = \frac{4Q}{\pi R^3}\left[\frac{1}{4}\left(\frac{\mathrm{d}\ln\gamma_{\text{a}}}{\mathrm{d}\ln\tau}\right)\right], \tag{1}$$

where γ_{c} is the corrected shear strain rate, Q is the flow rate, R is tube radius, τ is WSS and γ_{a} is the apparent shear strain rate (Eq. (2)) which is a first approximation of the wall shear strain rate and is defined as [7,22]:

$$\gamma_{\text{a}} = \frac{4Q}{\pi R^3}. \tag{2}$$

Final corrected dynamic viscosities (μ_{c}) (Eq. (4)) were derived through division of τ (Eq. (3)) by the corrected non-Newtonian wall shear strain rate (Eq. (1)):

$$\tau = \frac{\Delta P R}{2L}, \tag{3}$$

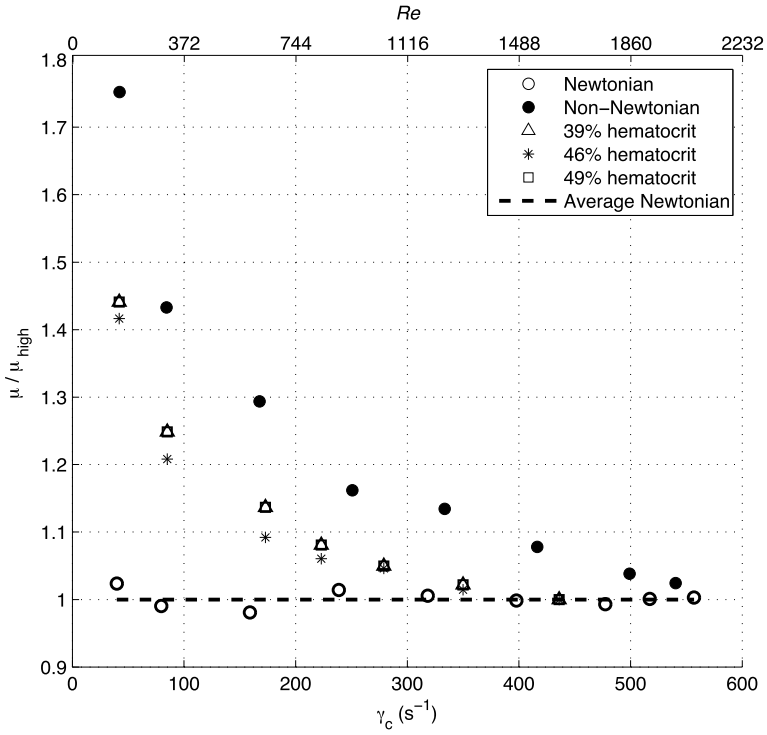

Fig. 1. Viscous behavior characterization of the Newtonian and non-Newtonian blood analog fluids through steady laminar pipe flow across a range of "corrected" shear strain rates (γ_c, bottom) and Reynolds number (*Re*, top). Viscosities were normalized to the respective high shear strain rate asymptotic viscosity (μ_{high}) of the non-Newtonian analog (μ/μ_{high}). Normalized values of blood viscosities at hematocrits of 39%, 46% and 49% to their respective high shear strain rate asymptotic viscosities are presented for reference [23]. Wall shear strain rates presented for the non-Newtonian analog fluid have been corrected using the Weissenberg–Rabinowitsch correction.

$$\mu_c = \frac{\tau}{\gamma_c}, \tag{4}$$

where ΔP is the measured pressure drop within a pipe with radius R and a length L over which pressure drop measurements were acquired. The ratios of normalized non-Newtonian dynamic viscosities relative to the high shear rate asymptotic viscosity (μ/μ_{high}) were plotted against both wall shear strain rate and *Re* (Fig. 1). The non-Newtonian fluid demonstrated a shear-thinning behavior and presented with a high shear strain rate dynamic viscosity of approximately 1.38 centipoise (cP) that closely matched the average dynamic viscosity of the Newtonian analog and the shear-thinning behavior of normalized viscosities of real blood at several hematocrits [23]. The shear strain rate dependent viscosity relationship of the xanthan gum analog was subsequently used as a curve fit correction to ensure matching *Re* between both fluids during steady and pulsatile pressure drop measurements in the laminar regime. For all subsequent measurements at $Re > 2000$, the dynamic viscosities of the two analogs were assumed equal.

2.2. Steady straight flow loop setup

A simplified *in vitro* closed flow loop that incorporated straight, rigid tubing was constructed to model the physiological circulatory system (Fig. 2). Analog fluids housed in an open reservoir were circulated

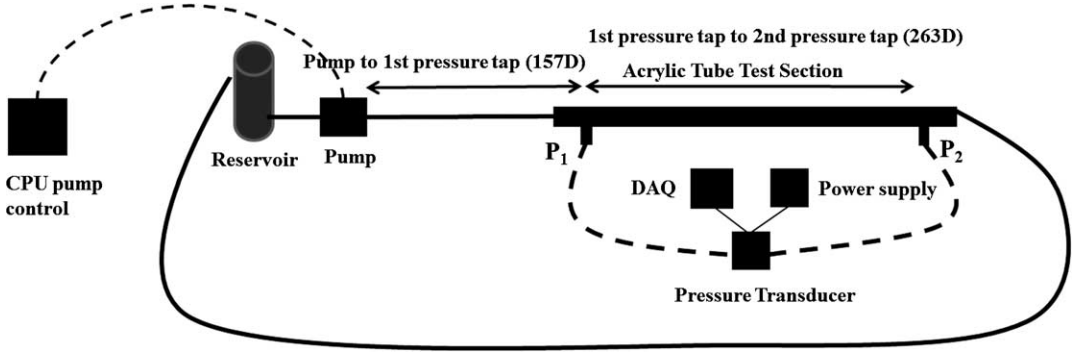

Fig. 2. Schematic of the flow loop for straight pressure drop measurements. Note that figure is not drawn to scale.

through the loop by an ISMATEC Reglo-Z digital gear pump (Cole Parmer, Montreal, QC, Canada) with a GJN-25 Micropump pump head (Cole Parmer). The test section consisted of a rigid, cylindrical acrylic tube (Laird Plastics, Calgary, AB, Canada) with a D of 0.635 cm and a total length of $288D$ representing an *in vitro*, unblocked artery. Pressure drops were measured by a calibrated Validyne model P305D differential pressure transducer (Northridge, CA, USA) between two pressure taps (P_1 and P_2) spaced $263D$ apart on the rigid tube. Pressure drops were acquired between $400 \leqslant Re \leqslant 7600$ at select intervals for both fluids equating to mean velocities between 0.085 m/s and 1.61 m/s respectively.

Measurements in the laminar regime were used to validate the experimental setup with Poiseuille's law. Moody diagrams were also constructed to display the relationship between *Re* and Darcy friction factor (f, Eq. (5)):

$$f = \frac{\Delta P}{\rho U^2}\frac{4R}{L}, \tag{5}$$

where ρ is the density of the working fluid, ΔP is the pressure drop required to drive the fluid through a pipe with length L and a radius R at an average velocity U. In laminar flow, the pressure drop is due to viscous dissipation within the fluid such that f decreases with increasing *Re* by the relationship $f = 64/Re$ [24]. For the turbulent regime, pressure drop is solely a function of pipe roughness whereupon the empirical Blasius relation of $f = 0.3164/Re^{1/4}$ holds [24].

The required entrance length (L_e) for fully-developed steady laminar flow (Eq. (6)) follows that suggested by Durst et al. [25]:

$$\frac{L_e}{D} = \left[(0.619)^{1.6} + (0.0567)^{1.6}\right]^{\frac{1}{1.6}}. \tag{6}$$

For non-Newtonian fluids, Poole and Ridley [26] concluded that the entrance lengths for Newtonian and non-Newtonian fluids diverge at $Re < 10$. However, given that measurements were acquired at $Re \geqslant 400$, entrance length requirements for both fluids were assumed equal. Therefore, a $157D$ entrance length from the pump outlet to P_1 ensured fully-developed flow for both analogs.

2.3. Pulsatile measurements

The experimental setup used for pulsatile measurements remained unchanged from that used for steady flow measurements whereupon pressure drops were acquired between P_1 and P_2 spaced $263D$

apart on a rigid acrylic tube. Two sinusoidal flow waveforms of $\alpha = 4$ and 6 with a frequency range of 0.3 Hz $< f <$ 1.05 Hz were constructed using a custom designed program in NI LabView 2011 (National Instruments, Austin, TX, USA) to generate pulsatile flow at select intervals between $400 \leqslant Re \leqslant 5600$. Womersley numbers associated with the Newtonian fluid were calculated using a constant value of 1.38 cP. For the non-Newtonian analog at $Re < 2000$, α was determined using viscosities calculated from a viscosity/shear strain rate curve fit based on the viscous characterization of the non-Newtonian analog (see Fig. 1). For $Re > 2000$, a value of 1.38 cP was used. Reynolds numbers presented for pulsatile flow represent the time-averaged mean *Re* (Re_{m}). An oscillatory *Re* (Re_{os}) of plus or minus one-third of Re_{m} of the pulsatile flow was selected for all waveforms, which equated to peak Reynolds numbers (Re_{p}) between $530 \leqslant Re_{\mathrm{p}} \leqslant 7500$. Although a sinusoidal waveform represents a simplification of an *in vivo* pulsed flow, it was felt that the salient features of an arterial waveform could be captured with a flow waveform consisting of steady flow and a single harmonic [27]. The sampling frequencies were set at 100 times the specific frequency at each α in order to synchronize each cycle into 100 sampling points. During the experiments, it was found that the sinusoidal wave frequency resonated with the inherent vibration frequency of the pressure transducer. To account for this, measured pressure drops from 15 pulsatile cycles were averaged whereupon an average pressure drop (ΔP_{m}) across the waveform was calculated. An ideal low-pass filter was constructed using MATLAB R2010 software (MathWorks, Natick, MA) with a cut-off frequency set to 7 Hz that served to filter the ringing artifact associated with the pressure transducer.

2.4. Obstructed flow loop setup

To generate shear-layer-induced transition, a brass hex nipple (Swagelok, Germany) representing a simplified stenosis in the form of an abrupt step was threaded to the straight test section that formed a 44% area reduction (Fig. 3(a)) at a distance of $284D$ from P_1 (Fig. 3(b)). A second piece of acrylic pipe with a matching D to that of the straight test section was threaded to the hex nipple with an additional pressure tap (P_3) located a distance of $36D$ downstream from the outlet of the blockage. The distance between pressure taps P_1 and P_3 was $320D$ (Fig. 3). It should be noted that this model could only be considered as a very simplified arterial model. Limitations associated with this model are further discussed (see Limitations).

Both steady and pulsatile pressure drops at matching *Re* and α to previous unblocked steady and pulsatile measurements were acquired to quantify the total obstructed pressure drop between P_1 and P_3. The added pressure drop to the system as a result of blockage inclusion (minor loss) was calculated through a two-step process. Firstly, the acquired straight pressure drops between P_1 and P_2 were linearly increased by 21.5%, which represented the expected values had straight pressure drops been acquired between P_1 and P_3. Subsequently, the linearly-extended straight pressure drops were then subtracted from the total obstructed system pressure drops ($P_1 - P_3$) to quantify the added pressure drop as a result of blockage inclusion. The parameters and measurement techniques used in the obstructed flow loop were commensurate with the straight flow loop as described previously. Obstructed flow data are presented using both inlet Reynolds number (Re_{in}) (Eq. (7)) and obstructed Reynolds number (Re_{d}) (Eq. (8)) as defined below, which represent the *Re* prior to entering the obstruction and the *Re* of the flow within the obstruction, respectively:

$$Re_{\mathrm{in}} = \frac{\rho \bar{U}_{\mathrm{in}} D}{\mu_{\mathrm{c}}}, \tag{7}$$

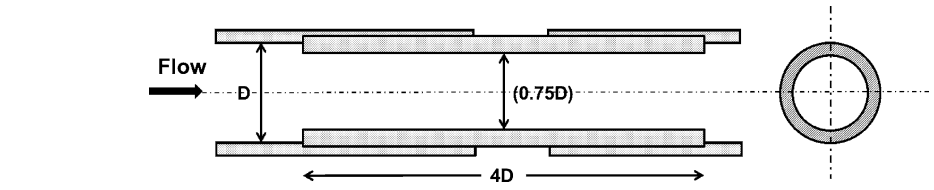

(a)

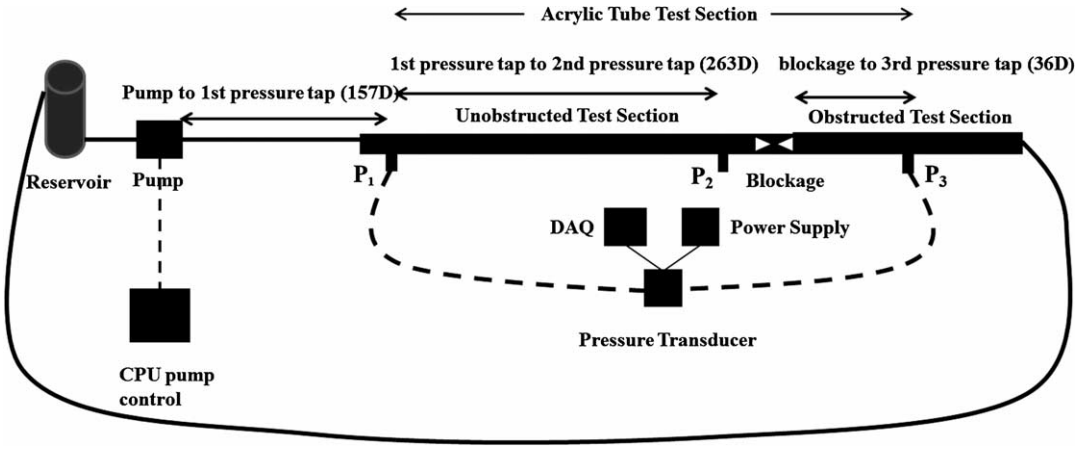

(b)

Fig. 3. Schematic of the added blockage (a) to the obstructed flow loop (b) for steady and pulsatile flow pressure drop measurements. Note that figure (b) is not drawn to scale.

$$Re_{\mathrm{d}} = \frac{\rho \bar{U}_{\mathrm{d}} d}{\mu_{\mathrm{c}}}, \tag{8}$$

where ρ is the density of the working fluids, $\bar{U}_{\mathrm{in}}$ and $\bar{U}_{\mathrm{d}}$ are the average inlet velocity and average velocity within the obstruction respectively, μ_{c} is the corrected dynamic viscosity (see Eq. (4)) and d is the diameter of the blockage equal to $0.75D$.

3. Results and discussion

3.1. Steady flow in straight flow loop

The transitional behaviors of the two analog fluids were first presented by plotting measured pressure drop as a function of *Re* (Fig. 4). Pressure drops for both analogs displayed a linear increase until $Re = 2200$. The Newtonian analog pressure drop deviated from the Poiseuille relationship at $Re > 2200$ (Fig. 4). This is in close agreement with the commonly accepted value of Re_{crit} for pipe flow, supporting the suitability of the current experimental work [24].

Measured pressure drop of the non-Newtonian analog followed the Poiseuille relation until $Re = 3200$, suggesting a delayed transition and prolonged laminar behavior in comparison to the Newtonian fluid (Fig. 5). This *Re* is in agreement with Han et al. [13], who reported that circulating porcine blood displayed laminar behavior up to $Re = 3200$ in steady flow. On a macroscale level, this finding supports

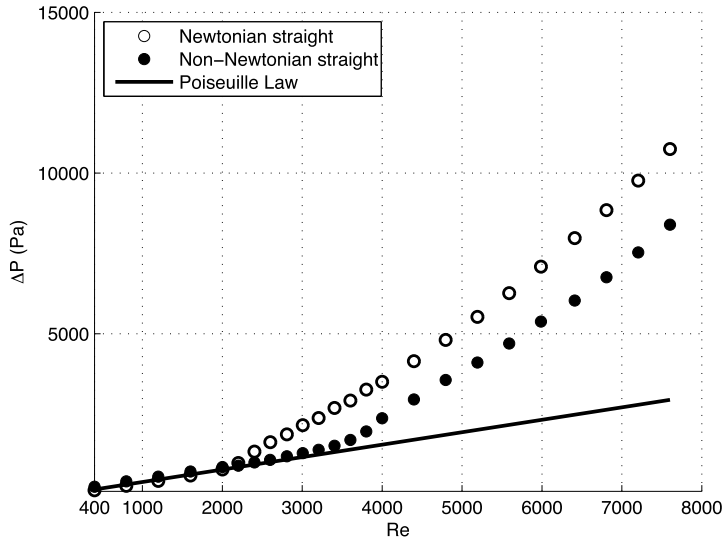

Fig. 4. Measured steady straight pressure drops (ΔP) between P_1 and P_2 as a function of *Re* for the Newtonian and non-Newtonian analogs. Theoretical values using Poiseuille law based on a $\mu = 1.38$ cP have been plotted for reference.

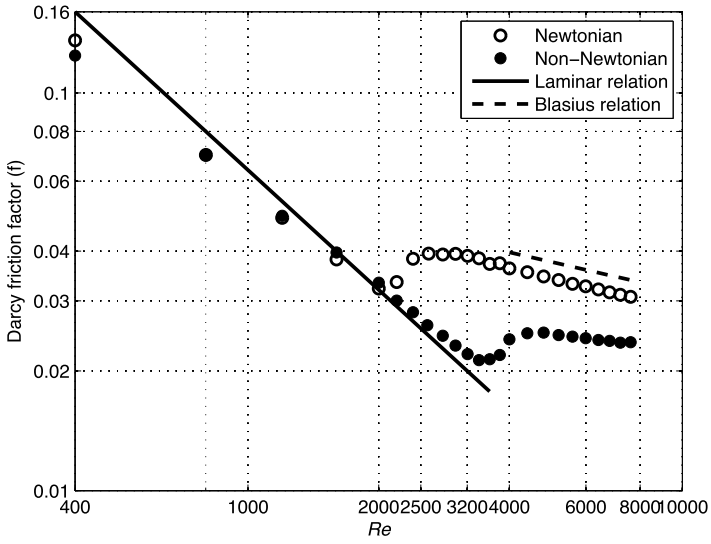

Fig. 5. Moody diagram for straight steady flow of Newtonian and non-Newtonian blood analogs where Darcy friction factor (f, Eq. (4)) is plotted against *Re*. The laminar Poiseuille relationship ($f = 64/Re$) and the turbulent Blasius relationship ($f = 0.3164/Re^{1/4}$) have been plotted for reference.

the suitability of using a xanthan gum blood analog to experimentally model transitional blood flow. It is speculated that the viscoelastic xanthan gum polymers serve to dampen turbulent bursts and delay transition through deformation and orientation of their long axis to the direction of flow. The measured delayed onset of transition also suggests that the concept of blood as a purely viscous fluid is inadequate to predict transitional and turbulent blood flow behavior.

3.2. Pulsatile flow in straight flow loop

The direct applicability of steady flow results to physiological problems is limited since blood flow in the large arteries is distinctly pulsatile. For pulsatile flow, plots of time-averaged mean pressure drop (ΔP_{m}) as a function of *Re* (Fig. 6) and Moody diagrams (Fig. 7) were constructed to directly evaluate the influence of pulsatile frequency on the transitional behaviors of both analogs.

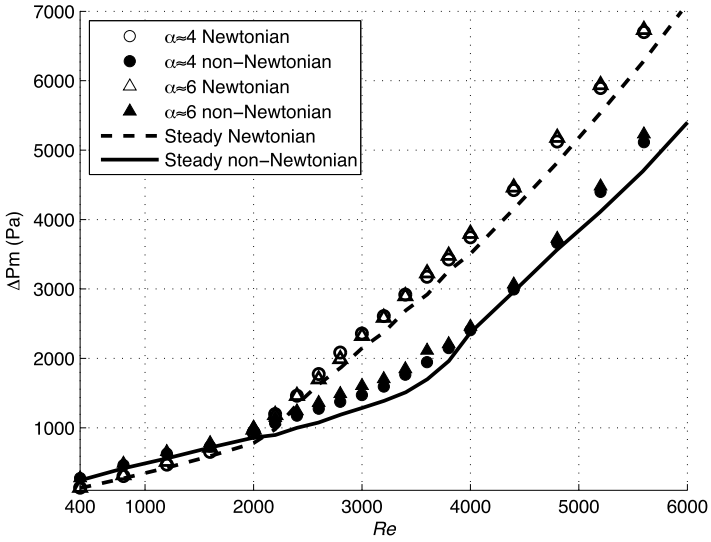

Fig. 6. Measured time-averaged straight mean pressure drops (ΔP_{m}) between P_1 and P_2 under pulsatile conditions at $\alpha = 4$ and 6 with reference to steady pressure drops for both analogs between P_1 and P_2.

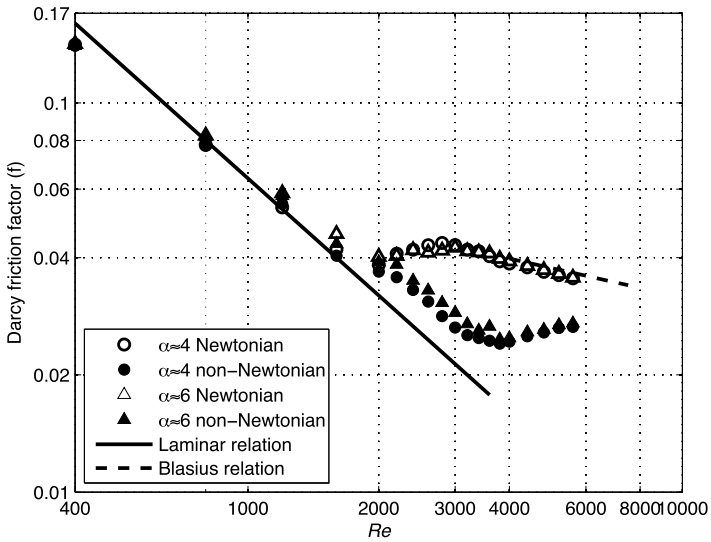

Fig. 7. Moody diagram for straight pulsatile flow of Newtonian and non-Newtonian blood analogs at Womersley numbers (α) of 4 and 6 where Darcy friction factor (f, Eq. (4)) is plotted against *Re*. The laminar relation ($f = 64/Re$) and turbulent Blasius relation ($f = 0.316Re^{-0.25}$) have been plotted for reference.

According to Hershey and Im [28], the addition of oscillations to steady flow increases the average flow resistance. This is observed in Fig. 6 whereupon the pulsatile pressure drop exceeds that of steady flow. Pulsatile Newtonian f increased linearly to $Re = 2000$, which suggested that transition was initiated between $2000 \leqslant Re \leqslant 2200$ (Fig. 8) [29]. This is in qualitative agreement with Çarpinlioğlu and Yaşar Gündoğdu [30] who estimated that the Re_{crit} for pulsatile flow was approximately 2100. Conversely, non-Newtonian f remained linear to $Re = 3800$ (Fig. 7).

Furthermore, the non-Newtonian analog in pulsatile flow transitioned at a higher Re_{crit} (3800) than in steady flow (3200), suggesting that the stability of pulsatile flow is further increased in comparison to steady flow for the non-Newtonian analog. Thurston and Pope [31] studied the laminar viscoelastic behavior of xanthan gum and suggested that the different relaxation times of the polymer were responsible for a higher pulsatile Re_{crit} in comparison to steady flow. It is suggested that unlike steady conditions, the pulsatile nature of the flow and constantly changing shear prevented the xanthan gum polymers from fully stretching. This allows the same amount of elastic energy stored in the polymers to dissipate more slowly and withstand a stable flow at a higher Re_{m} and subsequently Re_{crit} compared to steady flow.

On the other hand, results have shown negligible difference between steady, $\alpha = 4$ and 6 for each blood analog despite the different flow patterns. The importance of this observation implies that the steady component dictates the transition characteristics of unsteady flow. According to Trip et al. [17], clear conclusions regarding the relationship between transition and flows with Womersley numbers between 4–8 remains unclear. Further investigation and quantification of flows with these Womersley numbers certainly warrants further study.

3.3. Steady flow in obstructed flow loop

Calculated minor losses of both fluids as a result of the blockage addition were compared to expected theoretical values assuming an analogous area reduction using equations suggested by Seeley and Young [32] across the range of Re_{in} measured. Between $400 \leqslant Re_{\text{in}} \leqslant 3000$, calculated Newtonian and non-Newtonian minor losses were comparable to theoretical values (Fig. 8). However, it should be noted that the work of Seeley and Young [32] was restricted to a maximum $Re_{\text{in}} = 1000$ that equated to a Re_{d} of approximately 3700 based on a 93% area reduction using Newtonian glycerol–water mixtures compared to a 44% area reduction as was used here.

To demonstrate how pressure drops differed between the two fluids as a function of transitional mechanism (natural transition in a straight pipe vs. shear-layer-induced transition in an obstructed pipe), Newtonian to non-Newtonian pressure drop ratios for both straight and obstructed systems were calculated as:

$$\text{Percentage} = \left(\frac{\Delta P_{\text{Nt}}}{\Delta P_{\text{non-Nt}}} - 1 \right) \times 100\%, \tag{9}$$

where ΔP_{Nt} represents either the Newtonian minor loss, the straight P_1 to P_2 pressure drops or the obstructed P_1 to P_3 pressure drops and $\Delta P_{\text{non-Nt}}$ represents the corresponding non-Newtonian pressure drops. Straight system pressure drop ratios were higher at all $Re > 2000$ in relation to obstructed system pressure drops (Fig. 9). However, minor loss pressure drop ratios between the two fluids were comparable (Fig. 9). Previous studies have concluded that energy dissipation of downstream flow from a constriction is a function of the sudden expansion diameter [19,20]. Fratino and Pagano [21] concluded that the head loss coefficient was directly related to the energy dissipation of orifice plates of varying diameter reduction. Fratino and Pagano [21] found that a longer recirculation length, recirculation height

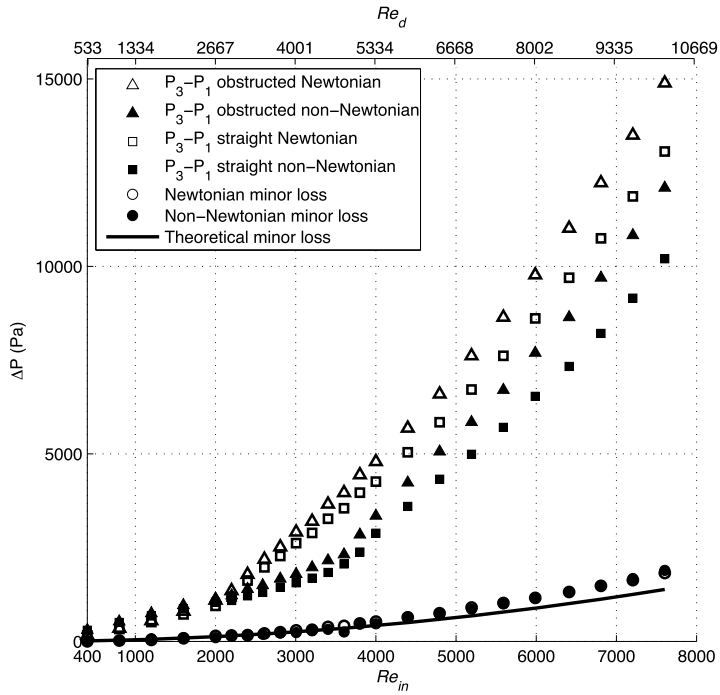

Fig. 8. Total obstructed system pressure drops between P_1 and P_3 (triangle), expected straight pressure drops between P_1 and P_3 (square) and minor losses due to the added obstruction (circle) of the Newtonian and non-Newtonian analog fluids. *Re* as presented in both Re_{in} (bottom) that was calculated using the diameter of the straight tube and Re_{d} (top), which was determined using the blockage diameter and expected average velocity within the blockage. Theoretical minor losses were calculated using equation provided by [32].

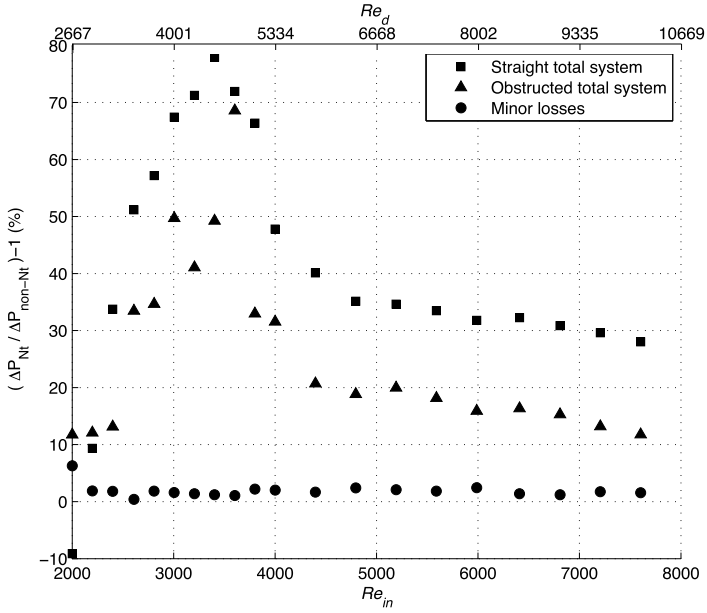

Fig. 9. Straight (square), obstructed (triangle) and minor loss (circle) pressure drop ratios between the Newtonian (ΔP_{Nt}) and non-Newtonian ($\Delta P_{\text{non-Nt}}$) analog fluids in steady flow.

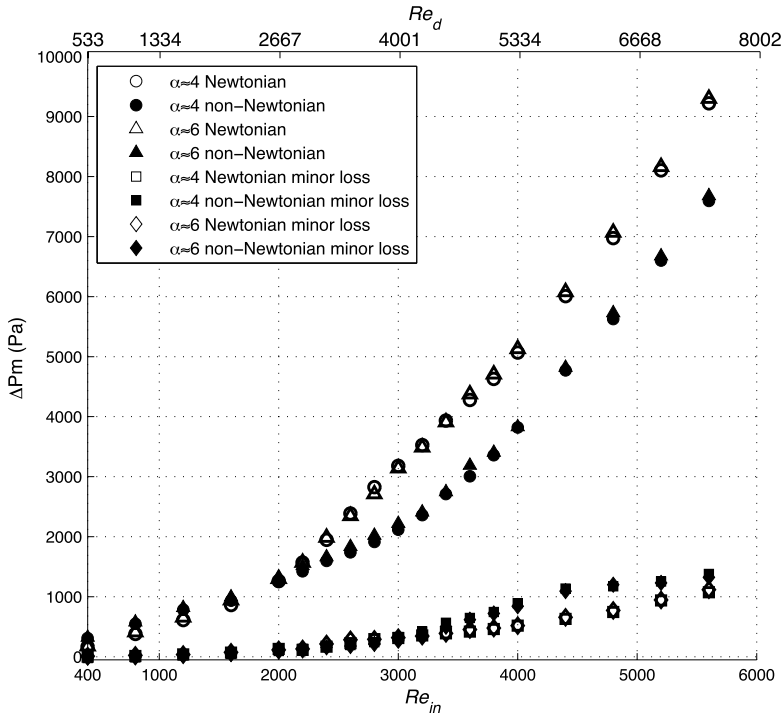

Fig. 10. Total obstructed system pressure drops between P_1 and P_3 and minor losses for Newtonian and non-Newtonian analog fluids at $\alpha = 4$ and 6.

and head loss were associated with orifice plates of greater diameter reductions. This suggests that the loss of mechanical energy is relevant to the recirculating flow region whereupon longer recirculation lengths lead to higher levels of energy dissipation. In non-Newtonian shear-layer-induced transitional flows, both Pak et al. [33] and Walker et al. [7] noted that the downstream recirculation length was extended in relation to Newtonian fluids. Although we cannot draw definitive conclusions, it is nonetheless proposed based on previous findings that the downstream post-blockage recirculation length of the xanthan gum analog was extended in relation to the Newtonian analog in transitional and turbulent flows.

Based on different pressure drop ratios between the obstructed and straight flow loops, our findings suggest that if one is simply using pressure drop to characterize blood flow, larger errors would be associated when using Newtonian assumptions in straight transitional flow. However, the reduced total pressure drop ratios in the obstructed system as a result of shear-layer-induced transition does not imply that substantial differences may exist in recirculation length, oscillatory shear indices (OSI) and WSS that are dependent on the fluid assumption used in shear-layer-induced transitional flow fields [7,14].

3.4. Pulsatile flow in obstructed flow loop

The total pulsatile obstructed system pressure drops of the non-Newtonian analog were lower than the Newtonian analog at $Re_{\text{in}} > 2200$, which is comparable to that observed in steady obstructed flow (Fig. 10). This agrees with Ikbal et al. [34] who used a viscoelastic model to represent a non-Newtonian fluid. Ikbal et al. [34] noted that the dimensionless pressure drop for viscoelastic fluids was less than Newtonian fluids at identical *Re* in pulsatile flow. Pontrelli [35] presented similar results showing a lower pressure drop across a blockage in pulsatile flow using non-Newtonian viscosity models. Minor

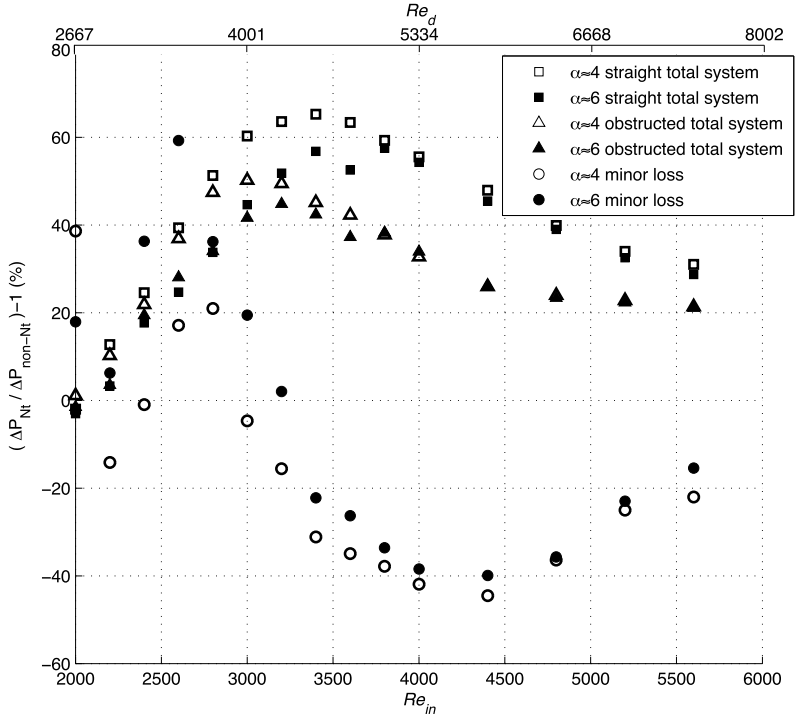

Fig. 11. Straight (square), obstructed (triangle) and minor loss (circle) pressure drop ratios between the Newtonian (ΔP_{Nt}) and non-Newtonian ($\Delta P_{\mathrm{non\text{-}Nt}}$) analog fluids at $\alpha = 4$ and 6.

loss ratios were found to be lower than steady obstructed minor loss ratios between $3400 \leqslant Re_{\mathrm{in}} \leqslant 5600$ at both α (Fig. 11). Based on an earlier argument, this would suggest a further extension of downstream recirculation length in pulsatile as compared to steady flow. It is speculated that multiple relaxation times as a function of varying shear strain rate across the pulsatile cycle served to stabilize pulsatile flow and contribute to increased pulsatile non-Newtonian minor losses in relation to steady flow conditions [31].

3.5. Physiological implications

The identification of turbulent flow and the conditions under which turbulent flow can exist in the cardiovascular system have long been of concern [36]. In healthy subjects, flow disturbances in the ascending aorta develop at peak velocity (0.71 m/s to 1.43 m/s) and persist into the decelerating phase [11]. However, in patients with aortic valve stenosis, the level of turbulence is approximately 10 times that observed in healthy subjects where peak velocities ranging from 3.08 to 4.59 m/s equating to a Re_{p} of approximately 10,000 have been measured [11]. Similar Re_{p} can be expected downstream of artificial heart valves [37]. Furthermore, in the presence of curvature, bifurcations and stenosis, turbulence can be generated at Re_{in} as low as a few hundred dependent on the severity of the constriction [9,38].

The average steady flow velocity at which pressure drop measurements were acquired ranged from $0.085 \text{ m/s} \leqslant U \leqslant 1.61 \text{ m/s}$ while peak pulsatile velocities ranged from $0.11 \text{ m/s} \leqslant U \leqslant 1.69 \text{ m/s}$. The maximum velocities of steady and pulsatile flow correspond to the physiological range of peak velocities observed in the ascending and descending aorta, patients with aortic valve stenosis or artificial mechanical heart valves and patients with severe arterial stenoses [37–40]. The obstructed model used

in the current study provided a first approximation to the physiological conditions where shear-layer-induced transition would develop downstream of a stenosis. Although progression of an arterial stenosis may be the result of turbulence, it likely has little effect on atherogenesis itself [41,42]. This is suggested by the results here, where through the use of aqueous xanthan gum as a blood analog, the deformation and flexibility of red blood cells may serve to delay transition and dampen the generation of disturbances in flow conditions normally believed to trigger transition. Therefore, use of a Newtonian assumption is likely to predict the onset of transitional behavior at a lower *Re* than may be occurring within the arterial system.

In large arteries where the internal diameter is much larger compared to the size of the red blood cell, blood can often be treated as a homogeneous Newtonian fluid with constant viscosity at all shear strain rates [41]. However, the results presented in this study have demonstrated the importance of non-linear viscous considerations in modeling transitional flows. It is proposed here, based on experience from past work, that the recirculation length was extended downstream of the blockage in transitional flow where the added viscoelastic polymer serves to dampen the generation of turbulent bursts. This suggests past work that has applied Newtonian assumptions to shear-layer-induced transitional flows (e.g. coarctations, stenoses) may have underestimated the extent to which downstream endothelium is exposed to recirculation. Post-blockage recirculation is characterized by low and oscillatory WSS that have been associated with atherogenic development. Regions of low and oscillatory WSS correspond to low nitric oxide production and enhanced arterial permeability, thus increasing the tendency for macro-molecules, including low density lipoprotein to accumulate within the intima [41]. However, due to the inverse relationship between shear strain rate and viscosity for shear-thinning fluids, higher WSS would be measured when using non-linear viscous as opposed to Newtonian viscous assumptions [6]. Based on this, use of a Newtonian assumption for blood may not only underestimate the length of recirculation, it may also underestimate WSS levels that could lead to an overestimate of detrimental consequences to homeostatic mechanisms.

4. Limitations

A number of simplifications were taken in this study to model physiological conditions. The compliance and natural curvature of the artery were neglected while physiological flow was represented by a sinusoidal waveform. Surface irregularities and asymmetry of *in vivo* stenoses were ignored through the use of an axisymmetric obstruction. Although past work has shown that the determination of Re_{crit} for transition is difficult due to the dependence on the specific geometry of the constriction [9,43,44], the use of an axisymmetric blockage does not diminish the validity or importance of this study. The simplified models provided a first approximation to the biological problem. The focus of this study was to highlight the importance of including the non-Newtonian behavior of blood in cardiovascular flow modeling by investigating the behavior of an analog fluid that presents with comparable shear-thinning behavior as a function of transition mechanism. Inclusion of additional non-linear physiological parameters such as compliance would add unneeded complexity that would hinder our ability to specifically isolate the contribution of non-Newtonian behavior on measured flow metrics.

5. Conclusions

Pressure drop measurements for a circulating non-Newtonian blood analog were acquired in both straight and obstructed *in vitro* simplified arterial models to quantify the influence of non-Newtonian

viscous behavior on transition initiation in comparison to a commonly used Newtonian analog. In general, it was found that the viscoelasticity of the non-Newtonian analog through the addition of an added polymer was likely responsible for the apparent difference in pressure drop relationships compared to the Newtonian analog. It is suggested here that this is analogous on a macroscale level to the behavior of red blood cells, which serve to prolong laminar flow behavior that has been reported previously.

Specifically, in a steady straight model, lower pressure drops were measured for the non-Newtonian analog in comparison to the Newtonian analog between $2200 \leqslant Re \leqslant 7600$, respectively. The Newtonian blood analog transitioned at a *Re* of approximately 2200 while the non-Newtonian blood analog displayed prolonged laminar flow behavior through $Re = 3200$. It is speculated that, analogous to red blood cells, the viscoelastic polymers in the non-Newtonian blood analog served to dampen turbulent bursts and reduce the generation of instabilities associated with natural transition. A possible mechanism responsible for the observed behavior is the storage of elastic energy within the entangled polymer. It is suggested that this stored energy was released in transitional flows under steady shear strain rates while the polymer orientated its long axis in the direction of flow, resulting in a lower pressure drop compared to the Newtonian analog.

The effect of pulsatile frequency on Re_{crit} for both fluids was negligible and suggests that further quantification is needed to draw broader conclusions in this range of α. Pulsatile non-Newtonian pressure drops, similar to steady pressure drops, were lower than the Newtonian analog at $Re \geqslant 2200$. Furthermore, the non-Newtonian analog in pulsatile flow presented with a higher Re_{crit} compared to that observed in steady flow. It is speculated that the different relaxation times of the polymer as a function of shear strain rate allowed for a slower release of elastic energy, thus stabilizing pulsatile flow to a larger Re_{crit}.

Calculated minor losses between for each of the two fluids in steady flow were comparable upon the addition of an obstruction to generate shear-layer-induced transition. Conversely in pulsatile constricted flow, non-Newtonian minor losses were greater than Newtonian minor losses. Although not directly quantified, it is proposed based on previous studies that an extended non-Newtonian recirculation length downstream of the obstruction is responsible for the comparable minor losses between the two fluids. It is speculated that the extension of downstream recirculation serves to reduce the generation of shear-layer-induced instabilities. For pulsatile flows, a further elongation of non-Newtonian recirculation length likely occurred whereupon non-Newtonian minor losses exceeded Newtonian minor losses between $3400 \leqslant Re_{\text{in}} \leqslant 5600$ at both α measured. The increased stability (e.g. higher Re_{crit}) observed in non-Newtonian pulsatile flow likely contributed to the elongation of recirculation in the obstructed system to a higher Re_{in} than that observed in steady flow leading to the increased minor losses. These findings could have far-reaching effects on blood flow modeling, which relies on Newtonian assumptions for the viscous behavior of blood, whereupon the extent of downstream shear-layer-induced recirculation may be underestimated.

References

[1] Pielhop K, Klaas M, Schröder W. Analysis of the unsteady flow in an elastic stenotic vessel. Eur J Mech-B/Fluids. 2012;35:102.

[2] Gijsen F, Van de Vosse F, Janssen J. The influence of the non-Newtonian properties of blood on the flow in large arteries: steady flow in a carotid bifurcation model. J Biomech. 1999;32:601.

[3] Mejia J, Mongrain R, Bertrand OF. Accurate prediction of wall shear stress in a stented artery: Newtonian versus non-Newtonian models. J Biomech Eng. 2011;133:074501.

[4] Schirmer CM, Malek AM. Wall shear stress gradient analysis within an idealized stenosis using non-Newtonian flow. Neurosurgery. 2007;61:853.
[5] Cavazutti M, Atherton MA, Collins MW, Barozzi GS. Non-Newtonian and flow pulsatility effects in simulation models of a stented intracranial aneurysm. Proc Inst Mech Eng Part H. 2011;225:597.
[6] Walker AM, Johnston CR, Rival DE. The quantification of hemodynamic parameters downstream of a Gianturco Zenith stent wire using Newtonian and non-Newtonian analogue fluids in a pulsatile flow environment. J Biomech Eng. 2012;134:111001.
[7] Walker AM, Johnston CR, Rival DE. On the characterization of a non-Newtonian blood analog and its response to pulsatile flow downstream of a simplified stenosis. Ann Biomed Eng. 2014;42:97.
[8] Fuster V, Topol EJ, Nabel EG. Atherothrombosis and coronary artery disease. Philadelphia: Lippincott Williams & Wilkins; 2005.
[9] Young DF, Tsai FY. Flow characteristics in models of arterial stenoses – I. Steady flow. J Biomech. 1973;6:395.
[10] Yee A, Bosworth KA, Conway DE, Eskin SG, McIntire LV. Gene expression of endothelial cells under pulsatile non-reversing vs. steady shear stress; comparison of nitric oxide production. Ann Biomed Eng. 2008;36:571.
[11] Stein PD, Sabbah HN. Turbulent blood flow in the ascending aorta of humans with normal and diseased aortic valves. Circ Res. 1976;39:58.
[12] Vétel J, Garon A, Pelletier D. Lagrangian coherent structures in the human carotid artery bifurcation. Exp Fluids. 2009;46:1067.
[13] Han S-I, Marseille O, Gehlen C, Blümich B. Rheology of blood by NMR. J Magnetic Reson. 2001;152:87.
[14] Molla MM, Paul MC. LES of non-Newtonian physiological blood flow in a model of arterial stenosis. Med Eng Phys. 2012;34:1079.
[15] Razavi A, Shirani E, Sadeghi M. Numerical simulation of blood pulsatile flow in a stenosed carotid artery using different rheological models. J Biomech. 2011;44:2021.
[16] Brookshier K, Tarbell J. Evaluation of a transparent blood analog fluid: aqueous xanthan gum/glycerin. Biorheology. 1993;30:107.
[17] Trip R, Kuik D, Westerweel J, Poelma C. An experimental study of transitional pulsatile pipe flow. Phys Fluids. 2012;24:014103.
[18] Stettler J, Hussain A. On transition of the pulsatile pipe flow. J Fluid Mech. 1986;170:169.
[19] Bullen P, Cheeseman D, Hussain L. The effects of inlet sharpness on the pipe contraction pressure loss coefficient. Int J Heat Fluid Flow. 1988;9:431.
[20] Fossa M, Guglielmini G. Pressure drop and void fraction profiles during horizontal flow through thin and thick orifices. Exp Thermal Fluid Sci. 2002;26:512.
[21] Fratino U, Pagano A. Head loss coefficient of orifice plate energy dissipator. J Hydraulic Res. 2011;49:830.
[22] Tickner EG, Sacks AH. Engineering simulation of the viscous behavior of whole blood using suspensions of flexible particles. Circ Res. 1969;25:389.
[23] Valant AZ, Žiberna L, Papaharilaou Y, Anayiotos A, Georgiou GC. The influence of temperature on rheological properties of blood mixtures with different volume expanders – implications in numerical arterial hemodynamics simulations. Rheol Acta. 2011;50:389.
[24] White FM. Fluid mechanics. New York: McGraw-Hill; 2010.
[25] Durst F, Ray S, Ünsal B, Bayoumi O. The development lengths of laminar pipe and channel flows. J Fluids Eng. 2005;127:1154.
[26] Poole RJ, Ridley BS. Development-length requirements for fully developed laminar pipe flow of inelastic non-Newtonian liquids. J Fluids Eng. 2007;129:1281.
[27] O'Rourke MF, Kelly RP, Avolio AP. The arterial pulse. Philadelphia: Lea & Febiger; 1992.
[28] Hershey D, Im CS. Critical Reynolds number for sinusoidal flow of water in rigid tubes. AIChE Journal. 1968;14:807.
[29] Ohmi M, Iguchi M, Urahata I. Flow patterns and frictional losses in an oscillating pipe flow. Bull JSME. 1982;25:536.
[30] Çarpinlioğlu MO, Yaşar Gündoğdu M. A critical review on pulsatile pipe flow studies directing towards future research topics. Flow Meas Instrument. 2001;12:163.
[31] Thurston GB, Pope GA. Shear rate dependence of the viscoelasticity of polymer solutions: II. Xanthan gum. J Non-Newt Fluid Mech. 1981;9:69.
[32] Seeley BD, Young DF. Effect of geometry on pressure losses across models of arterial stenoses. J Biomech. 1976;9:439.
[33] Pak B, Cho YI, Choi SU. Separation and reattachment of non-Newtonian fluid flows in a sudden expansion pipe. J Non-Newt Fluid Mech. 1990;37:175.
[34] Ikbal MA, Chakravarty S, Sarifuddin, Mandal PK. Unsteady analysis of viscoelastic blood flow through arterial stenosis. Chem Eng Comm. 2012;199:40.
[35] Pontrelli G. Blood flow through an axisymmetric stenosis. Proc Inst Mech Engineers Part H: J Eng Meg. 2001;215:1.
[36] Yellin EL. Laminar-turbulent transition process in pulsatile flow. Circ Res. 1966;19:791.

[37] Browne P, Ramuzat A, Saxena R, Yoganathan AP. Experimental investigation of the steady flow downstream of the St. Jude bileaflet heart valve: a comparison between laser Doppler velocimetry and particle image velocimetry techniques. Ann Biomed Eng. 2000;28:39.
[38] Pedley T, Schroter R, Seed W. The mechanics of the circulation. Cambridge: Cambridge Univ Press; 2011.
[39] Balducci A, Grigioni M, Querzoli G, Romano G, Daniele C, D'Avenio G, et al. Investigation of the flow field downstream of an artificial heart valve by means of PIV and PTV. Exp Fluids. 2004;36:204.
[40] Nguyen V-T, Kuan YH, Chen PY, Ge L, Sotiropoulos F, Yoganathan AP. Experimentally validated hemodynamics simulations of mechanical heart valves in three dimensions. Cardiovasc Eng Tech. 2012;3:88.
[41] Nichols WW, O'Rourke MF. McDonald's blood flow in arteries: theoretical, experimental, and clinical principles. 5th ed. Oxford: Taylor & Francis; 2011.
[42] Pedley TJ. The fluid mechanics of large blood vessels. Cambridge: Cambridge Univ Press; 1980.
[43] Young DF, Tsai FY. Flow characteristics in models of arterial stenoses – II. Unsteady flow. J Biomech. 1973;6:547.
[44] Vétel J, Garon A, Pelletier D, Farinas M. Asymmetry and transition to turbulence in a smooth axisymmetric constriction. J Fluid Mech. 2008;607:351.